

RESEARCH

Open Access



# Facile synthesis of degradable DOX/ICG co-loaded metal–organic frameworks for targeted drug release and thermoablation

Bei Liu<sup>1</sup>, Xiaoning Liu<sup>1</sup>, Xiangyu Zhang<sup>3</sup>, Xi Wu<sup>1</sup>, Chuanbo Li<sup>1</sup>, Zhaogang Sun<sup>2\*</sup> and Hongqian Chu<sup>2\*</sup>

\*Correspondence:  
sunzaogang@bjkyy.cn;  
chuhongqian@bjkyy.cn

<sup>1</sup> College of Science,  
Minzu University of China,  
Beijing 100081, China

<sup>2</sup> Translational Medicine Center,  
Beijing Chest Hospital, Capital  
Medical University/Beijing  
Tuberculosis and Thoracic  
Tumor Research Institute,  
Beijing 101149, China

<sup>3</sup> Laser Micro/Nano-Fabrication  
Laboratory, School of Mechanical  
Engineering, Beijing Institute  
of Technology, Beijing 100081,  
China

## Abstract

**Background:** Despite the increasing interest in combination therapy for the treatment of cancer, controlled delivery of different therapeutics with high body-clearance efficacy and cancer cell specificity remained a great challenge. In this study, a novel codelivery system was synthesized through one-pot coordination-driven self-assembly of 2-methylimidazole, zinc ion and chemotherapeutic drug (doxorubicin, DOX), followed by a surface decoration of photothermal agent (indocyanine green, ICG). To improve the targeting specificity performance, folic acid-conjugated polyethylene glycol (FA-PEG) antennas was connected on the surface of nanoparticles.

**Results:** The hybrid nanoparticles keep stable under neutral physiological condition but decompose when exposed to acidic environment, resulting in the on-demand release of DOX and ICG for chemo-photothermal combined therapy. Moreover, by switching the initial large size (~94 nm) to an ultrasmall size (~10 nm) in cancer cells, the nanoparticles hold great potential to avoid nanotoxicity for clinical applications.

**Conclusions:** This work provides a new strategy for co-delivery of different therapeutics for combined cancer therapy with high cancer cell specificity and low nanotoxicity.

**Keywords:** Metal–organic frameworks, Co-delivery nanosystem, Tumor specificity, Degradable

## Introduction

Metal–organic frameworks (MOFs) are micro-porous materials synthesized by self-assembly of organic linkers with metal or metal-oxo nodes (Lian et al. 2017; Bai et al. 2016; Simon-Yarza et al. 2018; Kalaj et al. 2020; Giliopoulos et al. 2020; Meng et al. 2020; Yang et al. 2020; Zhang et al. 2020). When scaled down to the nano-scale, MOFs can serve as efficient nanocarriers for drug delivery, thanks to their unique characteristics, such as high surface area, suitable size, well-defined channels and tailorabile chemistry (Wankar et al. 2020; Wang et al. 2019; Sun et al. 2020; Gao et al. 2021; Zhong et al. 2020). Researchers have either taken advantage of the porous structure of MOFs to load them with drugs, or developed new modification/encapsulation technologies for the effective



© The Author(s) 2022. **Open Access** This article is licensed under a Creative Commons Attribution 4.0 International License, which permits use, sharing, adaptation, distribution and reproduction in any medium or format, as long as you give appropriate credit to the original author(s) and the source, provide a link to the Creative Commons licence, and indicate if changes were made. The images or other third party material in this article are included in the article's Creative Commons licence, unless indicated otherwise in a credit line to the material. If material is not included in the article's Creative Commons licence and your intended use is not permitted by statutory regulation or exceeds the permitted use, you will need to obtain permission directly from the copyright holder. To view a copy of this licence, visit <http://creativecommons.org/licenses/by/4.0/>. The Creative Commons Public Domain Dedication waiver (<http://creativecommons.org/publicdomain/zero/1.0/>) applies to the data made available in this article, unless otherwise stated in a credit line to the data.

drug loading in MOFs. Despite exhaustive efforts, drug resistance induced by prolonged monotherapy still remains a formidable challenge.

To overcome this, much effort has been devoted to develop MOF-based co-delivery nanosystems. Different anti-tumor agents can be co-loaded in a single MOF to overcome drug resistance and improve the therapeutic efficiency. Lin and coworkers (He et al. 2014) reported the first example of MOFs for the co-delivery of cisplatin and pooled small interfering RNAs, leading to an order of magnitude enhancement in chemotherapeutic efficacy. After that, many co-delivery strategies based on MOFs have been published (Ringaci et al. 2021; Rabiee et al. 2021; Jia et al. 2019; Kang et al. 2020; Liu et al. 2019). Our research group also reported a nanoscale MOF that can simultaneously encapsulate nucleic acid therapeutics and chemotherapeutic drugs through a biomimetic mineralization strategy (Liu et al. 2019). Although effective, the reported MOF-based co-delivery nanosystems can be efficiently taken up by the reticuloendothelial system, resulting in long-term retention and potential amplification of toxicity. The development of MOF-based nanosystem for controlled co-loading of different therapeutics with high body-clearance efficacy and tumor specificity is, therefore, highly desirable.

Here, we report a new kind of MOF-based nanotherapeutics that allows tumor-targeted co-delivery of a small-molecule drug and a photothermal agent to enhance therapeutic efficacy. The strategy involves the one-pot coordination-driven self-assembly of 2-methylimidazole, zinc ions and doxorubicin (DOX) to synthesize DOX-encapsulated MOF, followed by surface decoration with indocyanine green (ICG). Folic acid-conjugated polyethylene glycol (FA-PEG) antennas were then attached to the surface of the nanoparticles through coordination interactions, endowing the hybrid nanoparticles with an enhanced active targeting effect toward cancer cells (Yang et al. 2020; Shi et al. 2018; Hai et al. 2017). Notably, upon the active accumulation of nanoparticles into tumor cells through FA-receptor-mediated endocytosis, the MOFs dissociated. Consequently, the size of the hybrid nanoparticles decreased from the initial large size of 94 nm to an ultrasmall size of 10 nm, which is highly desirable due to their low cytotoxicity and fast systemic clearance. Furthermore, the cytotoxic effect of the hybrid nanoparticles with integrated therapeutic modalities of chemotherapy and thermoablation was investigated in detail. Overall, this study offers a new strategy to combine robust, smart MOFs with integrated flexibility and multifunctionality for enhanced tumor-specific therapy, thus highlighting new opportunities to develop next-generation smart nanomedicines for cancer therapy.

## Experimental

### Materials

Zn(NO<sub>3</sub>)<sub>2</sub>·6H<sub>2</sub>O and 2-methylimidazole were purchased from Sigma-Aldrich. ICG and methanol (99.5%) were purchased from Aladdin. DOX was bought from TCI. PEG-FA (molecular weight = 2000 Da) was provided by Shanghai Ponsure Biotech. Cell culture medium was bought from Wisent. Hoechst 33,258 and cell counting kit-8 (CCK-8) were purchased from Solarbio. Fetal bovine serum was bought from Wisent. Phosphate buffer solution (PBS) and Calcein AM/PI doublestain kit were bought from Yeasen. All chemicals were used as received without any further purification.

### Synthesis of DOX/Z-ICG-FA

DOX-loaded ZIF-8 nanoparticles were synthesized as following: 2 mL of 2-methylimidazole (284 mg/mL) and 0.2 mL of  $\text{Zn}(\text{NO}_3)_2 \cdot 6\text{H}_2\text{O}$  (148 mg/mL) were mixed with 1 mL of DOX (1 mg/mL). After stirring for 30 min at room temperature, the DOX-loaded ZIF-8 (labeled as DOX/Z) were collected by centrifugation (18,000 r/min, 10 min), washed with methanol, and redispersed in 5 mL of methanol. Then 1 mL of ICG solution (1 mg/mL) was added into DOX/Z solution. After stirring for 12 h, DOX/Z-ICG were collected by centrifugation.

The DOX/Z-ICG-FA were synthesized by the surface modification of PEG-FA on DOX/Z-ICG through the coordination interaction between FA and  $\text{Zn}^{2+}$ . Briefly, DOX/Z-ICG and PEG-FA were mixed in dimethyl sulfoxide (2 mL) and stirred for 48 h. After centrifugation and washed with dimethyl sulfoxide and deionized water, the as-synthesized DOX/Z-ICG-FA were redispersed in 5 mL of deionized water for future use.

### DOX release from DOX/Z-ICG-FA

DOX/Z-ICG-FA were dispersed in 2 mL of  $\text{pH}=7.4$  or 5.5 PBS under magnetic stirring. At the given time periods (e.g., 1 h, 2 h, 3 h, 5 h, 8 h, 12 h), the release media were collected by centrifugation. The precipitate was then redispersed in 2 mL of fresh media. The release amount of DOX was determined by a UV-Vis spectrophotometer (UV-3600, Shimadzu, Japan).

### Photothermal conversion of DOX/Z-ICG-FA

Aqueous suspensions of DOX/Z-ICG-FA with different concentrations (0, 5, 10 and 20  $\mu\text{g}/\text{mL}$ ) were prepared and irradiated with an 808 nm near-infrared light (NIR) laser ( $1.0 \text{ W cm}^{-2}$ ). The temperature of DOX/Z-ICG-FA solution was recorded using a thermal imaging camera (TiS65, Fluke, USA). The temperature of deionized water was used as control. The photothermal conversion efficiency of DOX/Z-ICG-FA was measured as following: DOX/Z-ICG-FA aqueous solution was irradiated with 808 nm light for 6 min. Then the laser was shut off. The solution temperature was recorded carefully. The time constant for heat transfer was determined by applying linear time data versus  $\ln \theta$  from the cooling stage.

### Cell culture and cellular uptakes

Human breast cancer cells (MCF-7) were cultured in essential media (DMEM, pH 7.0–7.4) supplemented with 10% fetal bovine serum, 100 units/ml aqueous penicillin G and 100  $\mu\text{g}/\text{mL}$  streptomycin. The cells were seeded into a glass bottom dish and cultured at 37 °C in a humidified atmosphere containing 21%  $\text{O}_2$  and 5%  $\text{CO}_2$  for 24 h. Then the cells were treated with a final concentration of 10  $\mu\text{g}/\text{mL}$  DOX/Z-ICG-FA for 2 h or 4 h incubation. After that, the cells were washed with PBS thrice to remove the excess nanoparticles. Finally, the cells were stained with Hoechst 33342, and imaged by Olympus Fluoview FV1000 confocal microscope (Olympus, Japan). Note

that the pinhole and gain setting of the confocal laser scanning microscopy (CLSM) were kept constant during imaging.

#### Cellular temperature monitoring

MCF-7 cells were seeded in 24-well microplates and cultured overnight. Fresh medium containing DOX/Z-ICG-FA was added and incubated for 4 h. Then the cells were washed with PBS. Fresh culture medium was added, followed by 808 nm NIR light irradiation ( $1.0 \text{ W/cm}^2$ ) for 6 min. The cell temperature was carefully recorded by a thermometer (TiS65, Fluke, USA).

#### CCK-8 assay

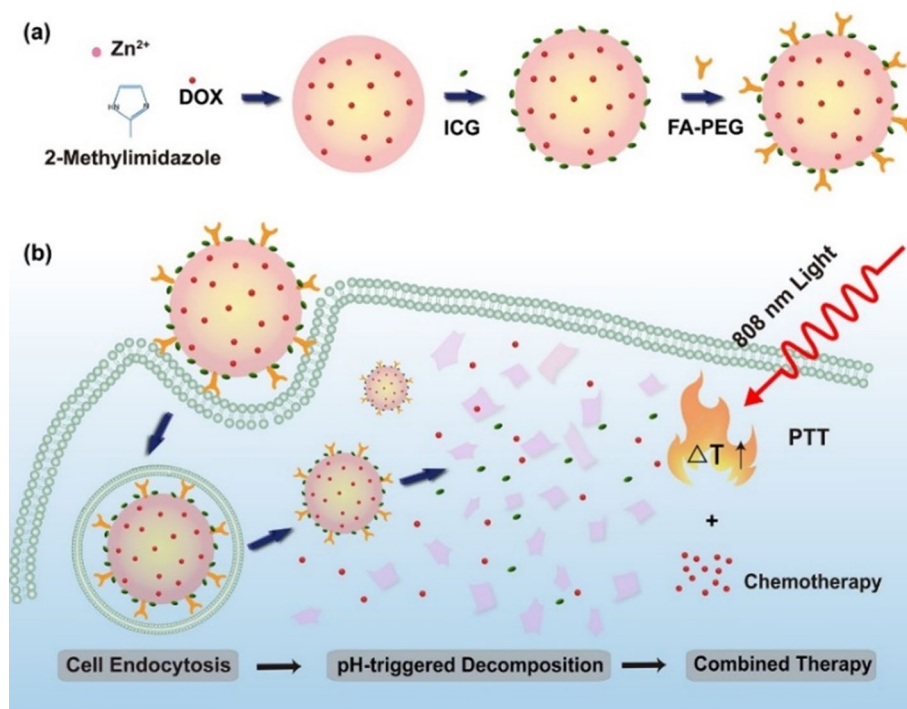
MCF-7 cells were seeded in 96-well microplates ( $8 \times 10^3$  cells/well) and cultured at  $37^\circ\text{C}$  in a humidified atmosphere containing 21%  $\text{O}_2$  and 5%  $\text{CO}_2$  for 24 h. Then fresh medium containing ZIF-ICG-FA, DOX/Z-ICG or DOX/Z-ICG-FA was added and incubated for 4 h. The cells were washed with PBS for three times before the irradiation with 808 nm NIR light ( $1.0 \text{ W/cm}^2$ , 6 min). After that, the cells were further incubated for another 24 h. 100  $\mu\text{L}$  of CCK-8 (10% in cell culture medium) was added to each well and incubated at  $37^\circ\text{C}$  for 1 h. The cytotoxicity of the nanomaterials was analyzed using a microplate reader (Multiskan GO, Thermo Scientific, USA).

#### Cell apoptosis assessment

To investigate the apoptosis of MCF-7 cells, cells were first seeded in 35 mm confocal dishes (NEST Biotechnology) at a density of  $3 \times 10^5$  cells per well for 24 h. Then the cells were treated with nanoparticles for 4 h. After that, the cells were washed with PBS three times, cultured with fresh medium, and irradiated with 808 nm NIR light for 6 min ( $1.0 \text{ W/cm}^2$ ). After another 24 h incubation, cells were stained with calcein AM/PI doublestain kit according to the manufacturer's instructions. Finally, the cells were imaged by Olympus Fluoview FV1000 confocal microscope. During imaging process, the pinhole and gain setting of the CLSM were kept constant.

## Results and discussion

The detailed therapeutic strategy using DOX/Z-ICG-FA is presented in Scheme 1. ZIF-8, a readily synthesized zeolitic imidazolate framework material, was chosen as drug delivery nanosystem due to its good biocompatibility, excellent structural porosity and high physical/chemical stability (Chen et al. 2014; Deng et al. 2019; Wang et al. 2019). The dynamic coordination interaction between  $\text{Zn}^{2+}$  and 2-methylimidazolate allows an effective encapsulation of nanoparticles or drug molecules, whereas their permanent structural porosity and high specific surface area offer opportunities for high loading of additional therapeutics, leading to a great potential for co-delivery capacity. Transmission electron microscopy (TEM) images showed that nanoscale ZIF-8 were successfully synthesized through a bottom-up approach (Fig. 1a), proving the synthesis feasibility of rhombic dodecahedral ZIF-8. A chemotherapeutic drug of DOX and photothermal agent of ICG were then loaded in ZIF-8 via encapsulation and surface coordination, respectively. To prolong the blood circulation time and enhance the active tumor-targeting effect of nanoparticles, FA-PEG was further functionalized on the surface of



**Scheme 1** Schematic illustration of **a** the synthesis process of DOX/Z-ICG-FA and **b** the bioapplication for cancer treatment

nanoparticles, resulting in the formation of DOX/Z-ICG-FA. TEM images in Fig. 1b–d showed that the DOX/ICG loading or FA-PEG modification did not change the rhombic dodecahedral morphology of ZIF-8. The powder X-ray diffraction pattern of DOX/Z-ICG-FA was the same as that of ZIF-8 (Fig. 1e), while the peak intensity decreased because of the partial loss of crystallinity arising from the DOX encapsulation and the surface modification of ICG or PEG-FA (Chen et al. 2018).

To verify the successful synthesis of DOX/Z-ICG-FA, a series of experiments were separately carried out. First, we evaluated the aqueous dispersity of the resultant nanoparticles by dynamic light scattering (DLS). As characterized in Fig. 1f, the hydrodynamic diameters of ZIF, DOX/Z, DOX/Z-ICG and DOX/Z-ICG-FA were 155 nm, 159 nm, 164 nm and 188 nm, respectively. The increase in the DLS diameters for DOX/Z-ICG and DOX/Z-ICG-FA is consistent with the presence of ICG and FA-PEG on the surface of ZIF-8. Note that the hydrodynamic diameters were larger than the size data from TEM due to the solvent effect in the hydrated state. Then, the UV–Vis–NIR absorption spectra of free DOX, free ICG, free FA, DOX/Z-ICG and DOX/Z-ICG-FA were analyzed. As shown in Fig. 1g, the absorption spectrum of DOX/Z-ICG exhibits the characteristic peaks of both DOX (450–600 nm) and ICG (600–850 nm), confirming the successful loading of DOX and ICG in DOX/Z-ICG nanoparticles. After the surface modification with FA-PEG, the absorption curve of DOX/Z-ICG-FA showed the characteristic peak of FA at ~300 nm, verifying the successful functionalization of FA on the surface of DOX/Z-ICG (Fig. 1h). The color change of DOX/Z-ICG dispersion can also verify the successful loading of DOX and

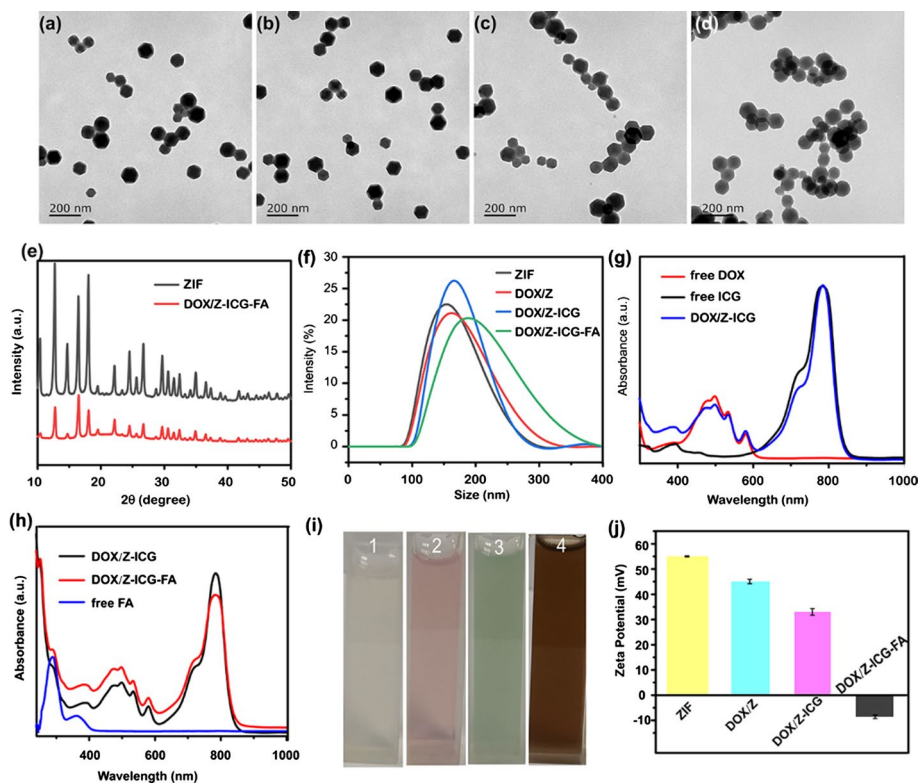


**Fig. 1** TEM images of **a** ZIF, **b** DOX/Z, **c** DOX/Z-ICG and **d** DOX/Z-ICG-FA. **e** PXRD of ZIF and DOX/Z-ICG-FA. **f** DLS of ZIF, DOX/Z, DOX/Z-ICG and DOX/Z-ICG-FA. **g** Absorption spectra of free DOX, free ICG and DOX/Z-ICG. **h** Absorption spectra of free FA, DOX/Z-ICG and DOX/Z-ICG-FA. **i** The photographs of 1: ZIF, 2: DOX/Z, 3: Z-ICG and 4: DOX/Z-ICG. **j** Zeta potentials of ZIF, DOX/Z, DOX/Z-ICG and DOX/Z-ICG-FA

ICG in nanoparticles (Fig. 1i). In addition, the surface zeta potential values changed from +55 mV to +45 mV after DOX encapsulation, yet turned to +33 mV after immobilization of ICG. After the attachment of FA-PEG, zeta potential decreased to -8.6 mV due to the carboxylic ions of PEG-FA (Fig. 1j).

The UV–Vis–NIR spectrum of DOX/Z-ICG possesses the characteristic peaks of ICG (Liu et al. 2016; Wan et al. 2019), thus exhibiting a strong absorption at 808 nm. With the increasing concentration of DOX/Z-ICG-FA, the absorption intensity at 808 nm increased obviously (Fig. 2a). These results motivated us to study the 808 nm-driven photothermal property of DOX/Z-ICG-FA. As depicted in Fig. 2b, the temperature elevation of DOX/Z-ICG-FA aqueous solution (20 μg/mL) increase to 71 °C under 808 nm laser irradiation (1.0 W/cm<sup>2</sup>), while water only increase to 25.2 °C, indicating that DOX/Z-ICG-FA nanoparticles can effectively convert the 808 nm NIR light to heat generation. The photothermal conversion efficiency ( $\eta$ ) of DOX/Z-ICG-FA was calculated as 23.5% (Fig. 2c). In addition, temperature increment of DOX/Z-ICG-FA remains high after 4 cycles of 808 nm laser irradiation, verifying the durable photothermal stability of DOX/Z-ICG-FA (Fig. 2d).

To test the thermal homogeneity of DOX/Z-ICG-FA solution (10 μg/mL), we used a thermal imaging camera to test the temperature below the laser irradiation position. As shown in Fig. 3, 1# (0 mm), 2# (10 mm), and 3# (20 mm) represent the temperatures at different distances from the laser irradiation. The results showed

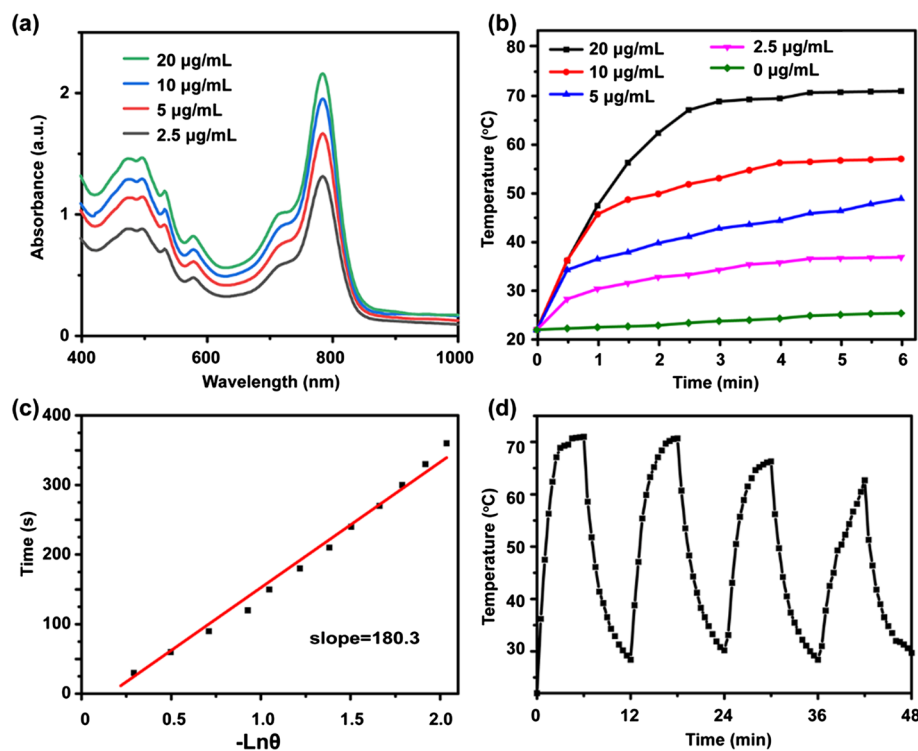


**Fig. 2** **a** Absorption spectra and **b** irradiation time-dependent temperature changes of different concentrations of DOX/Z-ICG-FA. **c** Plot of cooling time versus negative natural logarithm of the temperature driving force, obtained from the cooling curve of DOX/Z-ICG-FA. **d** Temperature changes of DOX/Z-ICG-FA over four ON/OFF irradiation cycles

similar temperature variation curves of 1#, 2# and 3#, suggesting the homogeneous temperature of DOX/Z-ICG-FA solution under the laser irradiation.

The controllable biodegradability and the long-term toxicity of nanoparticles have attached a lot of attention to their clinical applications. Therefore, it is highly desirable to exploit novel nanoagents that possess an appropriate dimension for effective cancer cell incubation, and satisfactory biodegradable property ensuring their harmless excretion from the body after the cancer therapy. As known, ZIF-8 can degrade in acidic environment of tumor cells ( $\text{pH} \sim 5.5$ ), while stay stable under normal physiological conditions ( $\text{pH} \sim 7.4$ ). Based on this line, we next studied the pH-responsive degradation of DOX/Z-ICG-FA by incubating DOX/Z-ICG-FA in PBS solutions with different pH values (pH 7.4 and 5.5). The results showed the as-synthesized DOX/Z-ICG-FA keep stable under neutral physiological condition, but decompose into small nanoparticles of  $\sim 10$  nm when exposed to acidic solution (Fig. 4a, b). The DOX release from DOX/Z-ICG-FA was also pH-dependent (Fig. 4c): the release amount of DOX reached 51.6% in pH 5.5 PBS at 12 h, much higher than that in pH 7.4 PBS (26.8%). Notably, 808 nm laser irradiation can effectively enhance the release amount of DOX owing to the increased temperature generated by ICG, which can accelerate the dissociation of DOX/Z-ICG-FA for DOX release.

The good performance of DOX/Z-ICG-FA in photothermal and drug release behavior motivated us to investigate their antitumor activity. First, the cellular uptake of

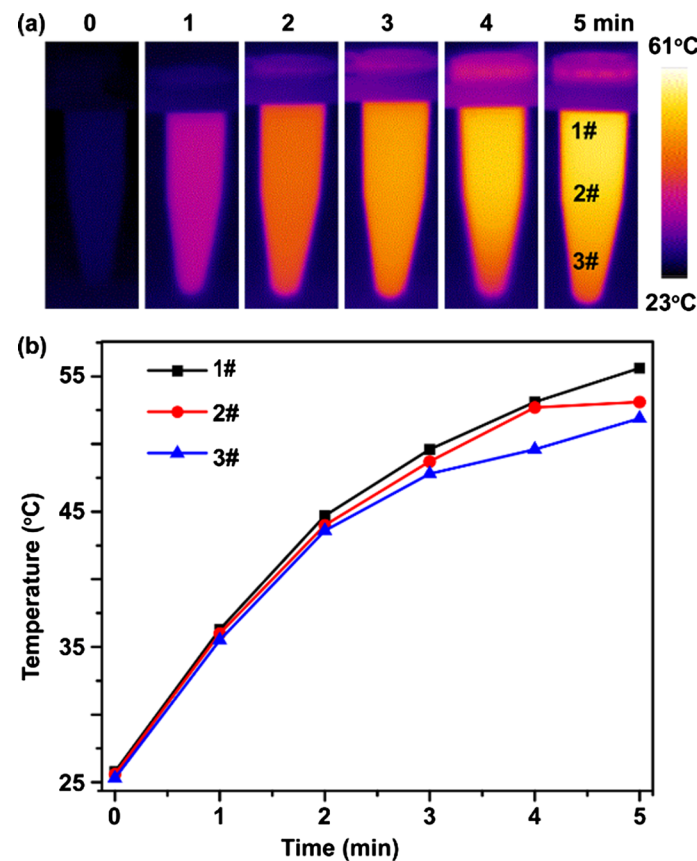


**Fig. 3** **a** Infrared thermal images and **b** temperature changes of DOX/Z-ICG-FA solution (10  $\mu\text{g}/\text{mL}$ ) under 808 nm laser irradiation. 1#, 2# and 3# represent the temperatures at different distances from laser irradiation (1#: 0 mm, 2#: 10 mm, 3#: 20 mm)

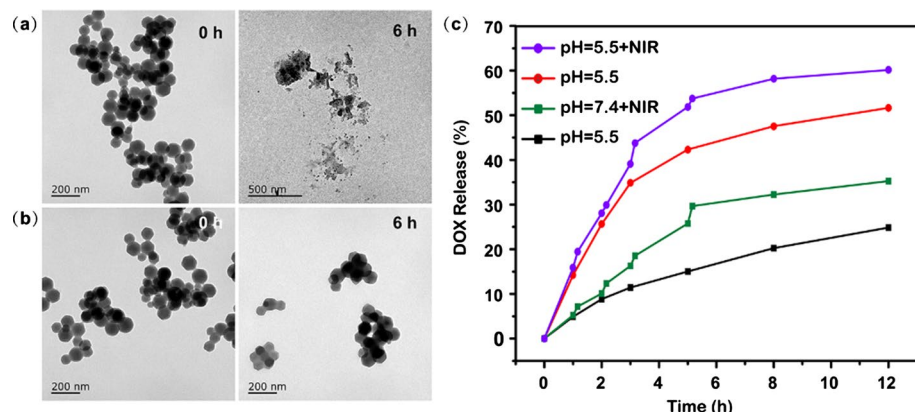


**Fig. 4** TEM images showing the pH-responsive decomposition of DOX/Z-ICG-FA in **a** pH = 5.5 PBS and **b** pH = 7.4 PBS. **c** DOX release profiles of DOX/Z-ICG-FA in PBS at pH 7.4 and 5.5 with/without 808 nm NIR irradiation

DOX/Z-ICG-FA was investigated by CLSM images. DOX/Z-ICG-FA were incubated with MCF-7 cells at 37  $^{\circ}\text{C}$  for 2 h and 4 h. The results in Fig. 5a showed bright fluorescence of DOX in cells, indicating the efficient internalization of DOX/Z-ICG-FA. Moreover, the fluorescence intensity of DOX increased with the treatment time, suggesting

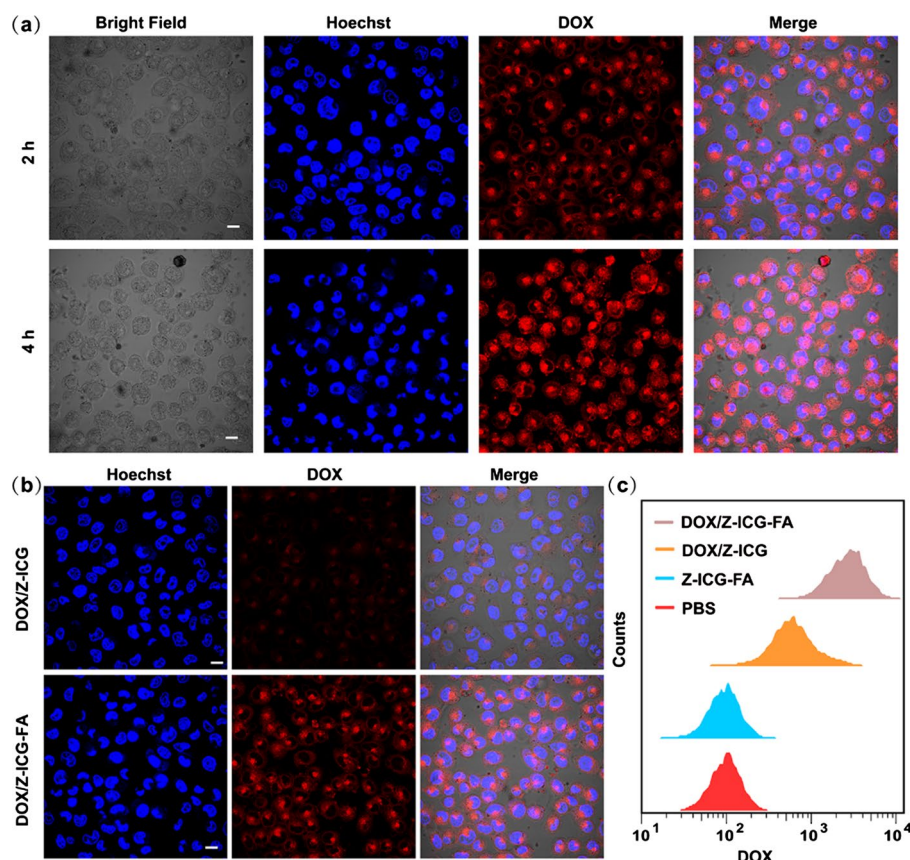


**Fig. 5** **a** Confocal fluorescence images of MCF-7 cells after cell incubation with DOX/Z-ICG-FA for 2 h and 4 h. Scale bars: 10  $\mu$ m. **b** Confocal fluorescence images of MCF-7 cells after cell incubation with DOX/Z-ICG or DOX/Z-ICG-FA for 4 h. The cell nuclei were stained with Hoechst 33342. Scale bars: 10  $\mu$ m. **c** Flow cytometric quantification of the cellular uptake of Z-ICG-FA, DOX/Z-ICG or DOX/Z-ICG-FA

an endocytosis-mediated uptake of DOX/Z-ICG-FA. The intracellular uptake efficiency of DOX/Z-ICG and DOX/Z-ICG-FA was also demonstrated. Figure 5b, c demonstrates that the cells treated with DOX/Z-ICG-FA showed more red-fluorescence signal of DOX than those treated with DOX/Z-ICG, indicating the enhanced cellular uptake of DOX/Z-ICG-FA via FA-receptor-mediated endocytosis.

To monitor the NIR-induced heating effect on tumor cells, the temperature of the cells was measured upon irradiation with 808 nm laser. As shown in Fig. 6, the cell temperature increased from 25 °C to 50.3 °C upon the 808 nm laser irradiation for 6 min, confirming the photothermal effect of DOX/Z-ICG-FA as anti-tumor agents. Then the cell cytotoxicity of DOX/Z-ICG-FA against MCF-7 cell line was evaluated. As shown in Fig. 7a, the cell viability did not decrease significantly when treated with NIR light irradiation, ZIF-ICG or ZIF-ICG-FA, indicating the negligible toxicity of these treatments to cells. Upon 808 nm NIR light irradiation, the excellent photothermal conversion ability of nanohybrids significantly improve the therapeutic efficacy against MCF-7. Notably, the cells treated with DOX/Z-ICG-FA following NIR irradiation led to the highest cell cytotoxicity (71.8%), achieving an enhanced potency through the combination of FA receptor-mediated targeting, chemotherapy and NIR-induced photothermal

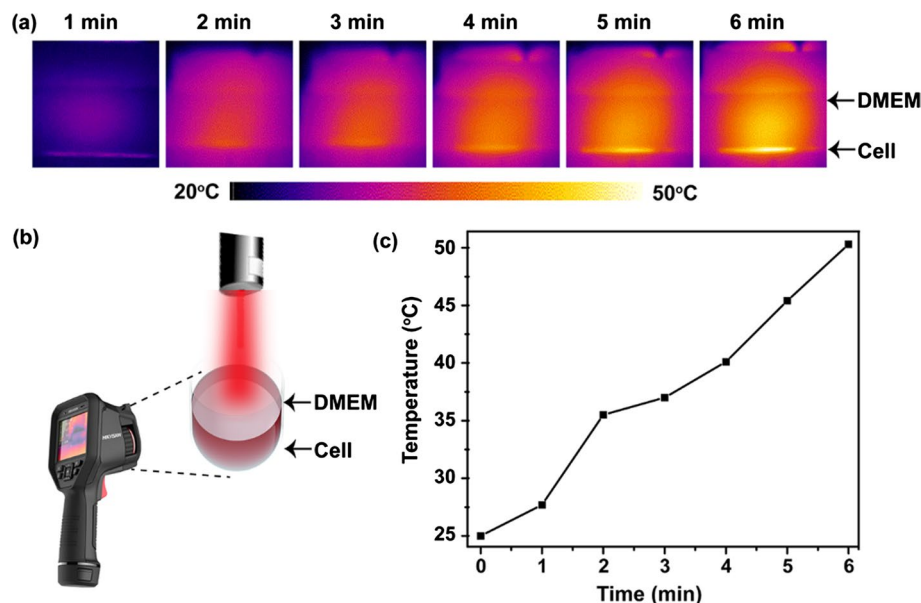


**Fig. 6** **a** Infrared thermal images of MCF-7 cells cultured in 24-well microplates upon irradiation with 808 nm laser. **b** Schematic illustration of the experimental devices for real-time monitoring of cell temperature. **c** Temperature changes of MCF-7 cells in (a) under 808 nm laser irradiation

therapy. The CCK-8 results were further supported by the AM/PI detection assay. As shown in Fig. 7b, MCF-7 cells in DOX/Z-ICG-FA + NIR group showed an apparent fluorescence change from green to red color, implying the efficient cell killing effect of DOX/Z-ICG-FA.

### Conclusions

To avoid nanotoxicity, we developed a novel degradable functional nanoparticle of DOX/Z-ICG-FA for synergistic combination of chemotherapy and photothermal therapy. The studies showed that the nanoparticles possess uniform size, high tumor-targeting specificity and pH-response degradability. The antitumor activity was evaluated on MCF-7 cells under different treatment conditions. The results indicated the DOX/Z-ICG-FA nanoparticles can enhance the targeting specificity to cancer cells, and have a high therapeutic effect (71.8%) in vitro. Therefore, the as-synthesized DOX/Z-ICG-FA nanoparticles is of great value for chemical and photothermal combined therapy in tumor treatment.

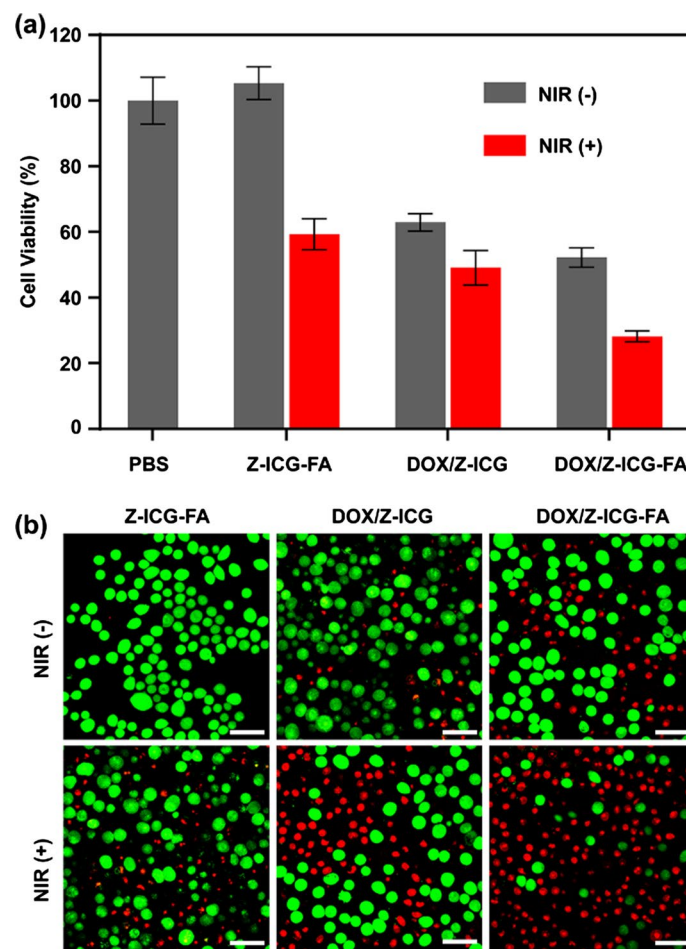


**Fig. 7** **a** Viability of MCF-7 cells after different treatments. **b** Confocal fluorescence images of cell apoptosis by staining with Annexin V-FITC and PI after different treatments. Scale bars: 50  $\mu$ m

#### Abbreviations

MOF	Metal–organic framework
DOX	Doxorubicin
ICG	Indocyanine green
ZIF-8	Zeolitic imidazolate framework-8
FA-PEG	Folic acid-conjugated polyethylene glycol
CLSM	Confocal laser scanning microscopy
CCK-8	Cell counting kit-8
PBS	Phosphate buffer solution
NIR	Near-infrared light
CLSM	Confocal laser scanning microscopy
TEM	Transmission electron microscopy
DLS	Dynamic light scattering
DMEM	Dulbecco's minimum essential medium
DOX/Z	DOX-loaded ZIF-8
DOX/Z-ICG	ICG-attached DOX/Z
DOX/Z-ICG-FA	FA-PEG attached DOX/Z-ICG

#### Acknowledgements

Not applicable.

#### Author contributions

All the authors contributed to the study conception and design. BL, XL and XW contributed to material preparation. BL, XL, XZ, XW, CL and HC conducted the experiments and collected the data. The first draft of the manuscript was written by BL and HC. All the authors reviewed the manuscript. All aspects of this study were supervised by HC and ZS. All authors read and approved the final manuscript.

**Funding**

This work was supported by the Natural Science Foundation of China (Nos. 82001946, 52105293, 61974170), Beijing Municipal Natural Science Foundation (No. 7214300).

**Availability of data and materials**

The data obtained in this study are provided in this manuscript. Further additional data can be provided by corresponding authors upon request.

**Declarations****Ethics approval and consent to participate**

Human cell lines used in this study do not require ethics approval.

**Consent for publication**

Not applicable.

**Competing interests**

The authors declare that they have no competing interests.

Received: 21 December 2021 Accepted: 12 May 2022

Published online: 06 June 2022

**References**

- Bai Y, Dou Y, Xie L, Rutledge W, Li J, Zhou H (2016) Zr-based metal-organic frameworks: design, synthesis, structure, and applications. *Chem Soc Rev* 45:2327–2367
- Chen X et al (2018) Derivative of epigallocatechin-3-gallate encapsulated in ZIF-8 with polyethylene glycol-folic acid modification for target and pH-responsive drug release in anticancer research. *ACS Biomater Sci Eng* 4:4183–4192
- Chen B, Yang Z, Zhu Y (2014) Zeolitic imidazolate framework materials: recent progress in synthesis and applications. *J Mater Chem A* 2:16811–16831
- Deng X et al (2019) Yolk-shell structured Au Nanostar@Metal-Organic framework for synergistic chemo-photothermal therapy in the second near-infrared window. *Nano Lett* 19:6772–6780
- Gao P, Chen Y, Pan W, Li N, Liu Z, Tang B (2021) Antitumor agents based on metal-organic frameworks. *Angew Chem Int Ed* 60:16763–16776
- Giliopoulos D, Zamboulis A, Giannakoudakis D, Bikiaris D, Triantafyllidis K (2020) Polymer/metal organic framework (MOF) nanocomposites for biomedical applications. *Molecules* 25:28
- Hai L et al (2017) Facile fabrication of a resveratrol loaded phospholipid/reduced graphene oxide nanoassembly for targeted and near-infrared laser-triggered chemo/photothermal synergistic therapy of cancer *in vivo*. *J Mater Chem B* 5:5783–5792
- He C, Lu K, Liu D, Lin W (2014) Nanoscale metal-organic frameworks for the co-delivery of cisplatin and pooled siRNAs to enhance therapeutic efficacy in drug-resistant ovarian cancer cells. *J Am Chem Soc* 136:5181–5184
- Jia Q et al (2019) A gamma-cyclodextrin-based metal-organic framework embedded with graphene quantum dots and modified with PEGMA via SI-ATRP for anticancer drug delivery and therapy. *Nanoscale* 11:20956–20967
- Kalaj M, Bentz KC, Ayala S, Palomba JM, Barcus KS, Katayama Y, Cohen SM (2020) MOF-polymer hybrid materials: from simple composites to tailored architectures. *Chem Rev* 120:8267–8302
- Kang Y et al (2020) Tetramodal imaging and synergistic cancer radio-chemotherapy enabled by multiple component-encapsulated zeolitic imidazolate frameworks. *ACS Nano* 14:4336–4351
- Lian X et al (2017) Enzyme-MOF (metal-organic framework) composites. *Chem Soc Rev* 46:3386–3401
- Liu B, Li C, Xing B, Yang P, Lin J (2016) Multifunctional UCNPs@PDA-ICG nanocomposites for upconversion imaging and combined photothermal/photodynamic therapy with enhanced antitumor efficacy. *J Mater Chem B* 4:4884–4894
- Liu B, Hu F, Zhang J, Wang C, Li L (2019) A biomimetic coordination nanoplatform for controlled encapsulation and delivery of drug-gene combinations. *Angew Chem Int Ed* 58:8804–8808
- Meng J et al (2020) Advances in metal-organic framework coatings: versatile synthesis and broad applications. *Chem Soc Rev* 49:3142–3186
- Rabiee N et al (2021) Polymer-coated NH<sub>2</sub>-UiO-66 for the codelivery of DOX/pCRISPR. *Acs Appl Mater Interfaces* 13:10796–10811
- Ringaci A, Yaremenko AV, Shevchenko KG, Zvereva SD, Nikitin MP (2021) Metal-organic frameworks for simultaneous gene and small molecule delivery *in vitro* and *in vivo*. *Chem Eng J* 418:129386
- Shi Z, Chen X, Zhang L, Ding S, Wang X, Lei QF, Fang W (2018) FA-PEG decorated MOF nanoparticles as a targeted drug delivery system for controlled release of an autophagy inhibitor. *Biomaterials Sci* 6:2582
- Simon-Yarza T, Mielcarek A, Couvreur P, Serre C (2018) Nanoparticles of metal-organic frameworks: on the road to *in vivo* efficacy in biomedicine. *Adv Mater* 30:15
- Sun Y et al (2020) Metal-organic framework nanocarriers for drug delivery in biomedical applications. *Nano-Micro Lett* 12:29
- Wan Y et al (2019) A biocompatible free radical nanogenerator with real-time monitoring capability for high performance sequential hypoxic tumor therapy. *Adv Funct Mater* 29:1903436
- Wang H, Chen Y, Wang H, Liu X, Zhou X, Wang F (2019) DNAzyme-loaded metal-organic frameworks (MOFs) for self-sufficient gene therapy. *Angew Chem Int Ed* 58:7380–7384
- Wankar J, Kotla NG, Gera S, Rasala S, Pandit A, Rochev YA (2020) Recent advances in host-guest self-assembled cyclodextrin carriers: Implications for responsive drug delivery and biomedical engineering. *Adv Funct Mater* 30:27

- Yang J, Dai D, Lou X, Ma L, Wang B, Yang Y (2020) Supramolecular nanomaterials based on hollow mesoporous drug carriers and macrocycle-capped CuS nanogates for synergistic chemo-photothermal therapy. *Theranostics* 10:615–629
- Zhang X et al (2020) A historical overview of the activation and porosity of metal-organic frameworks. *Chem Soc Rev* 49:7406–7427
- Zhong Y et al (2020) Recent advances in MOF-based nanoplates generating reactive species for chemodynamic therapy. *Dalton Trans* 49:11045–11058

#### Publisher's Note

Springer Nature remains neutral with regard to jurisdictional claims in published maps and institutional affiliations.

Ready to submit your research? Choose BMC and benefit from:

- fast, convenient online submission
- thorough peer review by experienced researchers in your field
- rapid publication on acceptance
- support for research data, including large and complex data types
- gold Open Access which fosters wider collaboration and increased citations
- maximum visibility for your research: over 100M website views per year

At BMC, research is always in progress.

Learn more [biomedcentral.com/submissions](https://biomedcentral.com/submissions)

